Approach to steady motion of a plate moving in a free-molecular gas under a constant external force

Kazuo Aoki,[1] Tetsuro Tsuji,[1] and Guido Cavallaro[2]
[1]*Department of Mechanical Engineering and Science, Kyoto University, Kyoto 606-8501, Japan*
[2]*Dipartimento di Matematica "G. Castelnuovo," Università di Roma "La Sapienza," 00185 Roma, Italy*
(Received 2 March 2009; revised manuscript received 6 May 2009; published 14 July 2009)

A thin plate accelerated or decelerated in a free-molecular gas at rest by a constant external force is considered. The force is in the direction perpendicular to the plate. In this situation, the plate velocity approaches its final constant velocity as time goes on. It is shown numerically that, under the diffuse-reflection boundary condition, the difference between the plate velocity and its final value decreases in proportion to an inverse power of time. This agrees with the previous theoretical result obtained under the assumption that the initial plate velocity is sufficiently close to the final one.

DOI: 10.1103/PhysRevE.80.016309 PACS number(s): 47.45.Dt, 47.45.Ab, 05.20.Dd, 51.10.+y

I. INTRODUCTION

In kinetic theory of gases, the two limiting cases, the continuum limit of vanishing Knudsen number (the mean free path of gas molecules divided by the characteristic length of the system) and the free-molecular limit of infinitely large Knudsen number, have been studied extensively. The former limit clarifies the relation between kinetic theory and fluid dynamics [1–6]. In the latter limit (free-molecular gas or Knudsen gas), the fact that the collision term of the Boltzmann equation can be neglected simplifies the analysis dramatically and the basic properties and phenomena appear to have been understood completely [2,3,6,7]. However, most of the existing works are devoted to steady flows of a gas or steady motions of a body and little is known about problems containing unsteady motion of a body (motion with acceleration, deceleration, or rotation of a nonsymmetric body). The difficulty in this case arises from the fact that, because of the absence of intermolecular collisions, the gas molecules impinging on the body may have a long memory and be affected by the trajectory of the body in the far past; i.e., there exists the effect of long memory. Indeed, this fact was mentioned already in Sec. H9 in [7]. However, to the best of the authors' knowledge, there is no systematic study of the effect. The present study, as well as the preceding studies [8–11], aims at clarifying the memory effect in the problems with an unsteady body motion by considering a simple problem of a body moving in a free-molecular gas with acceleration or deceleration. This is a numerical study complementing the previous mathematical works [8–11].

Let us consider a motion of a body in a uniform fluid (not a free-molecular gas) at rest caused by a constant external force. We assume that the body starts its motion with an initial velocity parallel to the external force and moves in the direction parallel to the external force without rotation because of a constraint or the symmetry of the body. A drag by the fluid acts on the body and its velocity approaches a constant value (final velocity) for which the drag counterbalances the external force. If we assume that the drag is proportional to the speed of the body, its velocity approaches the final velocity exponentially fast. That is, if we let τ be the time variable, $v_w(\tau)$ the velocity of the body in the direction of the external force, and $v_{w\infty}$ (>0) its final value, then for sufficiently large τ,

$$|v_{w\infty} - v_w(\tau)| \approx C_1 e^{-C_2\tau} \tag{1}$$

holds, where C_1 and C_2 are positive constants.

However, if the fluid is a free-molecular gas in an equilibrium state at rest, the manner of approach to the final velocity is quite different from Eq. (1) [8–11]. Let us assume that the body is a circular disk (with or without thickness) of dimension d $(d=1,2,3)$ and moves in the gas in the direction perpendicular to the disk. More specifically, the body is a real circular disk for $d=3$, an infinite plate with a finite width for $d=2$ and an infinite plate for $d=1$ (see Fig. 1; in [8,9,11] the gas molecules are assumed to move on the plane for $d=2$ and on the line for $d=1$, but there is no essential difference). In this case, the approach to the final velocity is slow and is proportional to an inverse power of time. That is, for sufficiently large τ,

$$|v_{w\infty} - v_w(\tau)| \approx C_1' \tau^{-n} \tag{2}$$

holds, where C_1' is a positive constant, and n is an integer, which depends on the dimension d of the disk and the model of gas-surface interaction. In [8,9], it was proven that $n=d+2$ when the gas molecules undergo specular reflection (or elastic collision) on the surface of the disk. The proof was extended to the case of a general convex body and it was shown that the same is true in this case [10]. Subsequently, it was shown in [11] that $n=d+1$ when the gas molecules undergo diffuse reflection (or reflection with complete accommodation). Moreover, as proven in [9] for the specular reflection, if the initial velocity v_{w0} (in the direction of the

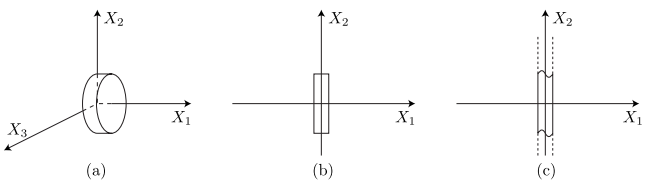

FIG. 1. A circular disk in a free-molecular gas. (a) Circular disk $(d=3)$, (b) infinite plate with a rectangular cross section $(d=2)$, and (c) infinite plate with a finite thickness $(d=1)$.

external force) is greater than the final velocity ($0 \leq v_{w\infty} < v_{w0}$), the disk velocity first decreases to a velocity smaller than the final one and then approaches it from below.

Law (2) is not exponential and this may appear somewhat surprising. The reason for this behavior is attributed to the presence of recollisions between the gas molecules and the disk. In fact, when it is accelerated, the disk can catch up with a gas molecule already hit by the disk and hit it again. In other words, the disk can hit the same molecule successively giving rise to a sequence of recollisions whose time intervals can be arbitrarily large. This creates a long tail memory, which is the cause of power law (2). In particular, in the presence of recollisions, the assumption to take a drag force proportional to the velocity of the disk is no more valid even when the velocity is small. If we ignore recollisions, for example, assuming that the disk always hits new molecules at a given thermal equilibrium, the behavior becomes that of Eq. (1). It is reasonable to expect that the effect of recollisions can be destroyed if the background is not a free-molecular gas but a gas with intermolecular collisions. In this case we can say that our result remains valid, not as a strict asymptotic behavior, but as a transient behavior. From an experimental point of view, it is delicate to observe such an effect and the authors are not aware of experiments in this direction. However, we should emphasize that the effect of recollision plays an important role when a body undergoes unsteady motion in a highly rarefied gas. It is also worth mentioning that it was already known that recollisions can produce a power-law decay. In fact the velocity-velocity correlation of a tagged particle of a one-dimensional (1D) free gas decays as τ^{-3} (see [12]).

The results in [8–11] described above have been proven under the condition that the initial velocity of the disk is sufficiently close to the final velocity, i.e.,

$$|v_{w\infty} - v_{w0}|/(2kT_0/m_*)^{1/2} \ll 1, \tag{3}$$

where T_0 is a reference temperature (e.g., the temperature of the ambient gas), k is the Boltzmann constant, and m_* is the mass of a molecule. Since this restriction is imposed by mathematical technicalities rather than physical situations, one cannot know how small it should be. In addition, the slow approach to the final steady motion is caused by the memory effect, so that it is not obvious whether the same results hold or not for an arbitrary initial velocity that does not satisfy Eq. (3). In the present study, therefore, we investigate this problem numerically and try to give a numerical evidence for the case of diffuse reflection. The reason why we restrict ourselves to the case of the diffuse reflection, rather than the specular reflection, will be explained in Sec. V D.

The origin of the problem of a specularly reflecting disk treated in Refs. [8,9] is explained from the point of view of particle dynamics in [8]. It should be remarked that the same problem has also been considered in connection with the so-called piston problem, which is a fundamental problem in statistical physics (see Refs. [13,14] and the references therein). For other types of obstacle-background interaction, the reader is referred to [15,16] (see also the references in [8–11]).

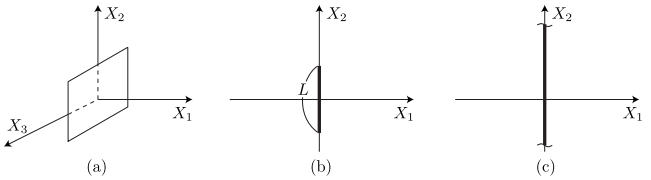

FIG. 2. A rectangular plate without thickness in a free-molecular gas. (a) Rectangular plate ($d=3$), (b) infinite plate with a finite width ($d=2$), and (c) infinite plate ($d=1$).

II. FORMULATION OF THE PROBLEM

A. Problem, assumptions, and notations

In the present study, we consider a rectangular plate of dimension d without thickness instead of a circular disk for convenience of the numerical analysis. That is, the body is a real rectangular plate for $d=3$, an infinite plate with a finite width for $d=2$, and an infinite plate for $d=1$ (Fig. 2). However, since the actual computation will be done mostly for $d=1$ and 2, we formulate the problem for the two-dimensional (2D) problem ($d=2$).

Let us consider an infinite expanse of an ideal gas in an equilibrium state at rest at temperature T_0 and density ρ_0. Suppose that an infinitely long plate with width L and without thickness, kept at temperature T_0, is fixed in the gas. Taking the X_1 axis perpendicular to the plate, the X_2 axis in the width direction, and the X_3 axis in the infinitely long spanwise direction, we assume that the plate is located at $X_1=0$, $-L/2 \leq X_2 \leq L/2$, and $-\infty < X_3 < \infty$ [Fig. 2(b)]. The plate is subject to a constant external force $\mathcal{F}(\geq 0)$ per unit mass in the direction of the positive X_1 axis. At $\tau=0$, the plate is released and launched with an initial velocity v_{w0} in the X_1 direction. Then, it moves along the X_1 axis and approaches the final steady motion with a constant velocity (final velocity). We investigate the motion of the plate, with special interest in the rate of approach to the final steady motion, under the following assumptions:

(i) The behavior of the gas is described by the Boltzmann equation [2,3,6].

(ii) The gas is so rarefied that the collisions between the gas molecules can be neglected (free-molecular gas or Knudsen gas) [2,3,6], and no external force acts on the gas molecules.

(iii) The gas molecules reflected on the plate are distributed according to the half-range Maxwellian distribution characterized by the temperature and velocity of the plate and there is no net mass flux across the plate (diffuse reflection) [2,3,6].

Before presenting the basic equations, we summarize the notations used in the paper. We first introduce (and repeat) dimensional quantities: the X_i is the Cartesian coordinate system in space, τ is the time variable, ξ_i is the molecular velocity, $X_w(\tau)$ is the position (X_1 coordinate) of the plate at time τ, $v_w(\tau)$ is the corresponding velocity (in the X_1 direction) of the plate, v_{w0} is the initial value of $v_w(\tau)$ at $\tau=0$, $v_{w\infty}$ is the final steady velocity of the plate $[v_{w\infty}=\lim_{\tau\to\infty} v_w(\tau)]$, $\tilde{f}(X_i, \xi_i, \tau)$ is the velocity distribution function of the gas molecules, $\mathcal{F}$ is the external force acting on the plate per unit

mass in the positive X_1 direction, $\mathcal{G}(\tau)$ is the drag acting on the plate per unit mass in the X_1 direction, and $\mathcal{M}$ is the mass of the plate per unit area. Then, we introduce the dimensionless counterparts x_i, t, ζ_i, x_w, u_w, u_{w0}, $u_{w\infty}$, f, F, G, and M by the following equations:

$$x_i = X_i/L, \quad t = \tau/\tau_0,$$

$$\zeta_i = \xi_i/(2kT_0/m_*)^{1/2}, \quad x_w(t) = X_w(\tau)/L,$$

$$u_w(t) = v_w(\tau)/(2kT_0/m_*)^{1/2}, \quad u_{w0} = v_{w0}/(2kT_0/m_*)^{1/2},$$

$$u_{w\infty} = v_{w\infty}/(2kT_0/m_*)^{1/2}, \tag{4}$$

$$f(x_i,\zeta_i,t) = \tilde{f}(X_i,\xi_i,\tau)/\rho_0(2kT_0/m_*)^{-3/2},$$

$$F = \mathcal{F}/L\tau_0^{-2}, \quad G(t) = \mathcal{G}(\tau)/L\tau_0^{-2},$$

$$M = \mathcal{M}/\rho_0 L,$$

where $\tau_0 = L(2kT_0/m_*)^{-1/2}$ is the reference time, k the Boltzmann constant, and m_* the mass of a gas molecule.

B. Basic equations

In the present spatially two-dimensional problem in which the physical quantities do not depend on x_3, we can eliminate the third component ζ_3 of the molecular velocity by considering the following marginal distribution function g:

$$g(x_1,x_2,\zeta_1,\zeta_2,t) = \int_{-\infty}^{\infty} f(x_1,x_2,\zeta_i,t)d\zeta_3. \tag{5}$$

Then, the Boltzmann equation for a free-molecular gas reads

$$\frac{\partial g}{\partial t} + \zeta_1\frac{\partial g}{\partial x_1} + \zeta_2\frac{\partial g}{\partial x_2} = 0. \tag{6}$$

The corresponding initial condition is

$$g = g_0, \quad g_0 = \pi^{-1}\exp(-\zeta_1^2 - \zeta_2^2), \quad (t=0), \tag{7}$$

and the boundary condition (diffuse reflection) on the plate is written as

$$g(x_1,x_2,\zeta_1,\zeta_2,t) = g_{w\pm}(x_2,\zeta_1,\zeta_2,t),$$

$$\left[x_1 = x_{w\pm}(t), -\frac{1}{2} \le x_2 \le \frac{1}{2}, \zeta_1 - u_w(t) \gtrless 0\right], \tag{8a}$$

$$g_{w\pm}(x_2,\zeta_1,\zeta_2,t) = \pi^{-1}\rho_{w\pm}(x_2,t)\exp(-[\zeta_1 - u_w(t)]^2 - \zeta_2^2), \tag{8b}$$

$$\rho_{w\pm}(x_2,t) = \mp 2\sqrt{\pi}\int_{-\infty}^{\infty}\int_{\zeta_1-u_w(t)\lessgtr 0}[\zeta_1 - u_w(t)] \times g(x_{w\pm}(t),x_2,\zeta_1,\zeta_2,t)d\zeta_1 d\zeta_2. \tag{8c}$$

Here, $x_1 = x_{w\pm}(t)$ indicates $x_1 = x_w(t) \pm 0$, so that $\{(x_1,x_2)\,|\,x_1 = x_{w\pm}, -1/2 \le x_2 \le 1/2\}$ stands for the surface of the plate facing to the positive x_1 axis (plus sign) or that facing to the negative x_1 axis (minus sign). In Eq. (8a)–(8c) and in what follows, the upper (or lower) signs go together.

The equation of motion of the plate is given as

$$dx_w(t)/dt = u_w(t), \quad du_w(t)/dt = F - G(t), \tag{9}$$

where the dimensionless drag $G(t)$ is expressed in terms of the velocity distribution function on the plate as follows:

$$G(t) = G_+(t) + G_-(t), \tag{10a}$$

$$G_\pm(t) = \pm\frac{1}{M}\int_{-1/2}^{1/2}\left\{\int_{-\infty}^{\infty}\int_{\zeta_1-u_w(t)\lessgtr 0}[\zeta_1 - u_w(t)]^2 \times g(x_{w\pm},x_2,\zeta_1,\zeta_2,t)d\zeta_1 d\zeta_2 + \int_{-\infty}^{\infty}\int_{\zeta_1-u_w(t)\gtrless 0}[\zeta_1 - u_w(t)]^2 \times g_{w\pm}(x_2,\zeta_1,\zeta_2,t)d\zeta_1 d\zeta_2\right\}dx_2. \tag{10b}$$

Here, $G_+(t)$ and $G_-(t)$ indicate, respectively, the drag acting on the surface at $x_{w+}(t)$ and $x_{w-}(t)$. The initial condition for Eq. (9) is

$$x_w(0) = 0, \quad u_w(0) = u_{w0}. \tag{11}$$

We are going to solve numerically the coupled systems, Eqs. (6), (7), and (8a)–(8c) and Eqs. (9), (10a), (10b), and (11).

In the spatially one-dimensional problem ($d=1$), in which the plate is an infinitely wide plate in the x_2x_3 plane and the physical quantities depend only on x_1, we can also eliminate the second component ζ_2 of the molecular velocity by introducing the marginal distribution function

$$\bar{g}(x_1,\zeta_1,t) = \int_{-\infty}^{\infty}\int_{-\infty}^{\infty} f(x_1,\zeta_i,t)d\zeta_2 d\zeta_3. \tag{12}$$

Therefore, the problem is much simpler. In this case, since there is no length scale related to the plate, we need to introduce an appropriate length scale (see Sec. V A). In the spatially three-dimensional problem ($d=3$), we have to handle the full distribution function $f(x_i,\zeta_i,t)$, so that the problem is more involved.

III. PRELIMINARIES

In this section, we transform Eqs. (6), (7), and (8a)–(8c) into integral equations for ρ_{w+} and ρ_{w-}, which are more convenient for numerical analysis.

The Boltzmann equation (6) indicates that g is constant along the characteristic line $x_\ell - \zeta_\ell t = \text{const}$ ($\ell = 1,2$), i.e., the projection of the molecular trajectory on the x_1x_2 plane. Let us consider the molecules impinging on the plate at time t, i.e., the molecules at $x_1 = x_{w+}$ (or $x_1 = x_{w-}$) and $-1/2 \le x_2 \le 1/2$ with $\zeta_1 - u_w(t) < 0$ [or $\zeta_1 - u_w(t) > 0$]. If we trace back the trajectories of such molecules reversing the time, we either (i) hit on the plate at a time in the past or (ii) reach the

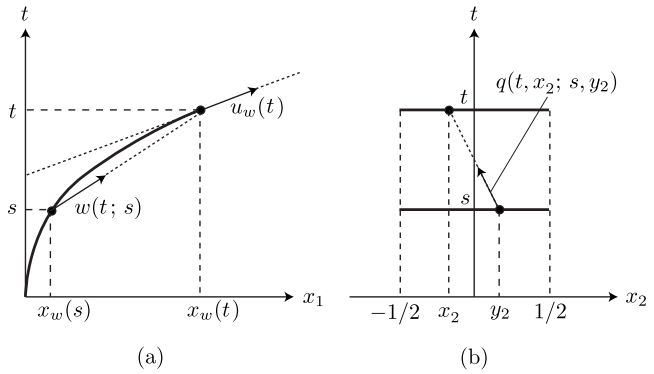

FIG. 3. Definitions of $w(t;s)$ and $q(t,x_2;s,y_2)$. (a) $w(t;s)$, (b) $q(t,x_2;s,y_2)$.

initial distribution g_0 at $t=0$ without hitting on the plate. The case (i) corresponds to the recollision mentioned in Sec. I. Taking this fact into account, we will express the right-hand side of Eq. (8c) in terms of g_0 and $g_{w\pm}$ (i.e., $\rho_{w\pm}$) in the past.

Let us suppose that a molecule that left the plate at point $(x_1,x_2)=(x_w(s),y_2)$ at time s in the past impinges on the plate again at point $(x_w(t),x_2)$ at time t. Here, we do not specify the side of the plate. Then, the x_1 and x_2 components of the velocity of the molecule, denoted by $w(t;s)$ and $q(t,x_2;s,y_2)$ respectively, are given by

$$w(t;s)=\frac{x_w(t)-x_w(s)}{t-s},\quad q(t,x_2;s,y_2)=\frac{x_2-y_2}{t-s},\qquad (13)$$

where $0\le s<t$, $-1/2\le y_2\le 1/2$ (Fig. 3). By definition, $\lim_{s\to t} w(t;s)=dx_w(t)/dt=u_w(t)$.

Let us assume that the trajectory of the plate $x_w(t')$ and the quantity $\rho_{w\pm}(x_2,t')$ in the boundary condition (8a)–(8c) are known for all $t'\in[0,t)$. The trajectory is depicted schematically in Fig. 4, where $x_1=x_w(t')$ is shown by the solid curve in the x_1t plane. The trajectory in the figure is exaggerated in order that the description of the solution method is facilitated. The projection on the x_1t plane of the trajectory of a molecule is a straight line, and the faster the molecule, the milder the slope of the line. Let us consider the molecules

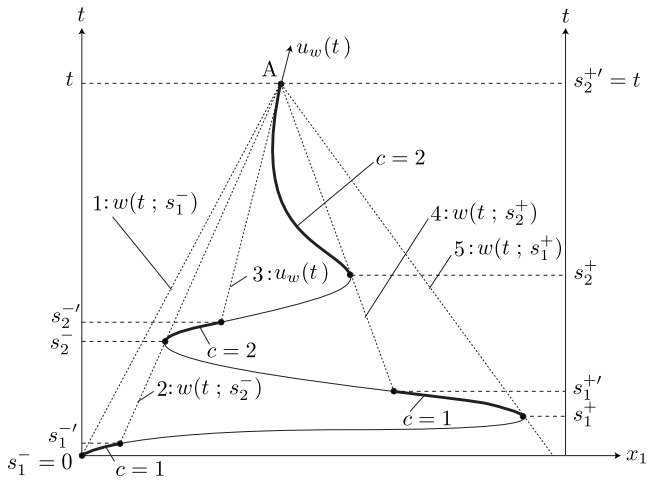

FIG. 4. Trajectory of the plate and definitions of the symbols.

impinging on the plate at point $(x_w(t),t)$, which is denoted by the symbol "A." An inclined straight line drawn downward from A indicates the trajectory of a molecule impinging on the plate at time t with a velocity (x_1 component) determined by the gradient of the line. More specifically, a line, such as line 5 in Fig. 4, located on the right-hand side of the tangential line at point A [line 3 in Fig. 4, the gradient of which corresponds to $u_w(t)$] stands for the trajectory of a molecule impinging on the right-hand face of the plate ($x_1=x_{w+}$, $-1/2\le x_2\le 1/2$), and a line, such as line 1 in the figure, located on the left-hand side of the tangential line stands for that of a molecule impinging on the left-hand face of the plate ($x_1=x_{w-}$, $-1/2\le x_2\le 1/2$).

We first consider the molecules impinging on the right-hand face of the plate. Let us consider the part of the trajectory of the plate (the solid curve in Fig. 4) located on the right-hand side of the tangential line at A. There are a finite number of segments of the trajectory that can be seen from point A without being hidden by the trajectory itself, which are numbered from below as $1,2,\ldots,n_+$ ($n_+=2$ in the case of Fig. 4). If there is no such segment, we set $n_+=0$. Let s_c^+ be the (dimensionless) time corresponding to the lower end of the cth segment, and $s_c^{+\prime}$ that corresponding to its upper end ($c=1,2,\ldots,n_+$). Then, the following relation holds when $n_+\ge 1$:

$$w(t;s_c^+)=u_w(s_c^+),\quad (c=1,2,\ldots,n_+),\qquad (14a)$$

$$w(t;s_c^+)<w(t;s_c^{+\prime})=w(t;s_{c+1}^+),\quad (c=1,2,\ldots,n_+-1).\qquad (14b)$$

Note that relation (14a) does not hold if $s_1^+=0$ [i.e., $w(t;0)\neq u_{w0}$].

We define the corresponding quantities also for the molecules impinging on the left-hand face of the plate. We consider the part of the trajectory of the plate, located on the left-hand side of the tangential line at A, and we number, as $1,2,\ldots,n_-$ from below ($n_-=2$ in the case of Fig. 4), the segments of the trajectory that can be seen from point A without being hidden by the trajectory itself. Let s_c^- be the time corresponding to the lower end of the cth segment, and $s_c^{-\prime}$ that corresponding to its upper end ($c=1,2,\ldots,n_-$). Then, the following relation holds when $n_-\ge 1$:

$$w(t;s_c^-)=u_w(s_c^-),\quad (c=1,2,\ldots,n_-),\qquad (15a)$$

$$w(t;s_c^-)>w(t;s_c^{-\prime})=w(t;s_{c+1}^-),\quad (c=1,2,\ldots,n_--1).\qquad (15b)$$

Note that relation (15a) does not hold if $s_1^-=0$ [i.e., $w(t;0)\neq u_{w0}$] (see Fig. 4).

With the help of s_c^+ and $s_c^{+\prime}$ defined above, the ρ_{w+} at point A, consisting of the contribution of the initial equilibrium distribution g_0 and that of g_{w+} in the boundary condition on the plate in the past, can be expressed as

$$\rho_{w+}(x_2,t) = -2\sqrt{\pi}\left\{\int_{-\infty}^{\infty}\int_{-\infty}^{u_w(t)}[\zeta_1 - u_w(t)]g_0(\zeta_1,\zeta_2)d\zeta_1 d\zeta_2 + \sum_{c=1}^{n_+}\int_{w(t;s_c^{+})}^{w(t;s_c^{+\prime})}\int_{q(t,x_2;s,1/2)}^{q(t,x_2;s,-1/2)}[\zeta_1 - u_w(t)] \times [g_{w+}(y_2,\zeta_1,\zeta_2,s) - g_0(\zeta_1,\zeta_2)]d\zeta_2 d\zeta_1\right\}, \quad (16)$$

where $\Sigma_{c=1}^{n_+}=0$ if $n_+=0$. In Eq. (16), s means $s(\zeta_1,t)$ determined implicitly by the first equation of Eq. (13) with $w=\zeta_1$, and y_2 means $y_2(x_2,\zeta_1,\zeta_2,t)$ determined by the second equation of Eq. (13) with $q=\zeta_2$ and $s=s(\zeta_1,t)$, i.e.,

$$\frac{x_w(t) - x_w(s(\zeta_1,t))}{t - s(\zeta_1,t)} = \zeta_1, \quad \frac{x_2 - y_2(x_2,\zeta_1,\zeta_2,t)}{t - s(\zeta_1,t)} = \zeta_2. \quad (17)$$

In Eq. (16), the first double integral on the right-hand side indicates the contribution if all the impinging molecules at time t come from the initial velocity distribution g_0. However, the impinging molecules whose velocity (ζ_1,ζ_2) is contained in the ranges of integration in the terms under summation $\Sigma_{c=1}^{n_+}$ departed from the plate in the past, not from the initial distribution. We call such molecules recolliding molecules and their effect the effect of recollision. The correction caused by the recolliding molecules is made by the terms contained in the summation $\Sigma_{c=1}^{n_+}$.

Similarly, ρ_{w-} is expressed in the form

$$\rho_{w-}(x_2,t) = 2\sqrt{\pi}\left\{\int_{-\infty}^{\infty}\int_{u_w(t)}^{\infty}[\zeta_1 - u_w(t)]g_0(\zeta_1,\zeta_2)d\zeta_1 d\zeta_2 + \sum_{c=1}^{n_-}\int_{w(t;s_c^{-\prime})}^{w(t;s_c^{-})}\int_{q(t,x_2;s,1/2)}^{q(t,x_2;s,-1/2)}[\zeta_1 - u_w(t)] \times [g_{w-}(y_2,\zeta_1,\zeta_2,s) - g_0(\zeta_1,\zeta_2)]d\zeta_2 d\zeta_1\right\}, \quad (18)$$

where $\Sigma_{c=1}^{n_-}=0$ if $n_-=0$, and s and y_2 mean $s(\zeta_1,t)$ and $y_2(x_2,\zeta_1,\zeta_2,t)$ determined by Eq. (17).

On the other hand, $G_+(t)$ and $G_-(t)$ in Eq. (10b) are recast as

$$G_+ = \frac{1}{M}\int_{-1/2}^{1/2}\left\{\int_{-\infty}^{\infty}\int_{-\infty}^{u_w(t)}[\zeta_1 - u_w(t)]^2 g_0(\zeta_1,\zeta_2)d\zeta_1 d\zeta_2 + \sum_{c=1}^{n_+}\int_{w(t;s_c^{+})}^{w(t;s_c^{+\prime})}\int_{q(t,x_2;s,1/2)}^{q(t,x_2;s,-1/2)}[\zeta_1 - u_w(t)]^2 \times [g_{w+}(y_2,\zeta_1,\zeta_2,s) - g_0(\zeta_1,\zeta_2)]d\zeta_2 d\zeta_1 + \int_{-\infty}^{\infty}\int_{u_w(t)}^{\infty}[\zeta_1 - u_w(t)]^2 \times g_{w+}(x_2,\zeta_1,\zeta_2,t)d\zeta_1 d\zeta_2\right\}dx_2, \quad (19)$$

$$G_- = -\frac{1}{M}\int_{-1/2}^{1/2}\left\{\int_{-\infty}^{\infty}\int_{u_w(t)}^{\infty}[\zeta_1 - u_w(t)]^2 g_0(\zeta_1,\zeta_2)d\zeta_1 d\zeta_2 + \sum_{c=1}^{n_-}\int_{w(t;s_c^{-})}^{w(t;s_c^{-\prime})}\int_{q(t,x_2;s,1/2)}^{q(t,x_2;s,-1/2)}[\zeta_1 - u_w(t)]^2 \times [g_{w-}(y_2,\zeta_1,\zeta_2,s) - g_0(\zeta_1,\zeta_2)]d\zeta_2 d\zeta_1 + \int_{-\infty}^{\infty}\int_{-\infty}^{u_w(t)}[\zeta_1 - u_w(t)]^2 \times g_{w-}(x_2,\zeta_1,\zeta_2,t)d\zeta_1 d\zeta_2\right\}dx_2, \quad (20)$$

where $\Sigma_{c=1}^{n_\pm}=0$ if $n_\pm=0$. The last integrals, containing $[\zeta_1-u_w(t)]^2\, g_{w\pm}(x_2,\zeta_1,\zeta_2,t)$ on the right-hand sides of Eqs. (19) and (20), indicate the contribution of the molecules leaving the plate at time t, whereas the other terms the contribution of the impinging molecules. The latter contribution consists, as in Eqs. (16) and (18), of the contribution of the initial velocity distribution and that of the molecules reflected by the plate in the past (recolliding molecules).

Equations (16) and (18), with the explicit form of $g_{w\pm}(y_2,\zeta_1,\zeta_2,s)$ in Eq. (8b), are the integral equations for ρ_{w+} and ρ_{w-}, respectively, to be solved together with Eqs. (9) and (10a) [with Eqs. (19) and (20)], and Eq. (11).

IV. NUMERICAL ANALYSIS

Let Δt be a small interval in t, $t_{(i)}=i\Delta t$ be the ith time step $(i=0,1,2,\ldots)$, and $x_{w(i)}$, $u_{w(i)}$, and $G_{(i)}$ be defined by

$$x_{w(i)} = x_w(t_{(i)}), \quad u_{w(i)} = u_w(t_{(i)}), \quad G_{(i)} = G(t_{(i)}). \quad (21)$$

Then, we discretize Eq. (9) as follows:

$$x_{w(i+1)} = x_{w(i)} + u_{w(i)}\Delta t, \quad (22a)$$

$$u_{w(i+1)} = u_{w(i)} + (F - G_{(i+1)})\Delta t, \quad (22b)$$

where $x_{w(0)}=0$ and $u_{w(0)}=u_{w0}$.

Suppose that $x_{w(j)}$, $u_{w(j)}$, and $g_{w\pm}$ (or $\rho_{w\pm}$) at $t=t_{(j)}$ are known for $j=0,1,2,\ldots,i$. Then, $x_{w(i+1)}$ is obtained from Eq. (22a). In order to obtain $u_{w(i+i)}$ from Eq. (22b), we need to compute $G_{(i+1)}=G_+(t_{(i+1)})+G_-(t_{(i+1)})$. This can be done by the use of Eqs. (19) and (20) if we have $g_{w\pm}$ (or $\rho_{w\pm}$) at $t=t_{(i+1)}$. We obtain the latter quantity using the discretized version of Eqs. (16) and (18), as explained below.

Let us consider Eq. (16) at $t=t_{(i+1)}$ and $x_2=x_{2(l)}$, where $x_{2(l)}=l\Delta x_2$ $(l=-N,\ldots,0,\ldots,N;\Delta x_2=1/2N)$. Thus, $(x_{w\pm}(t_{(i+1)}),x_{2(l)})$ is a discrete point on the plate at $t=t_{(i+1)}$. We first replace $u_w(t)(=u_{w(i+1)})$, which is unknown, on the right-hand side of Eq. (16) with $u_{w(i)}$ that is known. Then, the integrals containing g_0 can be reduced to expressions containing the error function, for which fast algorithms are available (see Sec. V D). The integrals containing g_{w+} are evaluated numerically using the discrete data in the past, i.e., $x_{w(j)}$, $u_{w(j)}$, and $\rho_{w+}(x_{2(l)},t_{(j)})$ $(j=0,1,\ldots,i;l=-N,\ldots,0,\ldots,N)$. With the explicit form of g_{w+} [Eq. (8b)], the integral containing g_{w+} under the summa-

tion in Eq. (16), after the replacement $u_{w(i+1)} \to u_{w(i)}$, is written as

$$\frac{1}{\pi}\int_{w(t;s_c^+)}^{w(t;s_c^{+'})}\int_{q(t,x_2;s,1/2)}^{q(t,x_2;s,-1/2)}[\zeta_1 - u_{w(i)}]\rho_{w+}(y_2,s) \times \exp(-[\zeta_1 - u_w(s)]^2 - \zeta_2^2)d\zeta_2 d\zeta_1,$$

$$(\text{at } t = t_{(i+1)},\ x_2 = x_{2(l)}), \tag{23}$$

where $s=s(\zeta_1,t)$ and $y_2=y_2(x_2,\zeta_1,\zeta_2,t)$ defined by Eq. (17). Let us suppose that $t_{(j)}(j=\alpha,\alpha+1,\ldots,\alpha') \in [s_c^+, s_c^{+'}]$ and $s_c^{+'} < t_{(\alpha'+1)}$. Since the trajectory $x_w(t)$ is approximated by straight line segments [Eq. (22)], $t_{(\alpha)}=s_c^+$ holds. Thus, Eq. (23) can be expressed as follows:

$$\frac{1}{\pi}\left(\sum_{j=\alpha}^{\alpha'-1}\int_{w(t;t_{(j)})}^{w(t;t_{(j+1)})} + \int_{w(t;t_{(\alpha')})}^{w(t;s_c^{+'})}\right)R(x_2,\zeta_1,t)Q(\zeta_1,t)d\zeta_1,$$

$$(\text{at } t = t_{(i+1)}, x_2 = x_{2(l)}), \tag{24}$$

where

$$R(x_2,\zeta_1,t) = \sum_{m=-N}^{N-1}\int_{q(t,x_2;s(\zeta_1,t),-m\Delta x_2)}^{q(t,x_2;s(\zeta_1,t),-(m+1)\Delta x_2)} P(x_2,\zeta_1,\zeta_2,t)d\zeta_2, \tag{25a}$$

$$Q(\zeta_1,t) = [\zeta_1 - u_{w(i)}]\exp(-(\zeta_1 - u_w(s(\zeta_1,t)))^2), \tag{25b}$$

$$P(x_2,\zeta_1,\zeta_2,t) = \rho_{w+}(y_2(x_2,\zeta_1,\zeta_2,t),s(\zeta_1,t))\exp(-\zeta_2^2). \tag{25c}$$

We first approximate $R(x_2,\zeta_1,t)$ and $u_w[s(\zeta_1,t)]$ in $Q(\zeta_1,t)$ by linear functions of ζ_1 in each range of integration in Eq. (24). Noting that $s(\zeta_1,t)=t_{(j)}$ and thus $u_w[s(\zeta_1,t)]=u_w[t_{(j)}] = u_{w(j)}$ for $\zeta_1=w(t;t_{(j)})$, we let

$$R(x_2,\zeta_1,t) = R(x_2,w(t;t_{(j)}),t) + [R(x_2,w(t;t_{(j+1)}),t) - R(x_2,w(t;t_{(j)}),t)]\frac{\zeta_1 - w(t;t_{(j)})}{w(t;t_{(j+1)}) - w(t;t_{(j)})}, \tag{26a}$$

$$u_w(s(\zeta_1,t)) = u_{w(j)} + [u_{w(j+1)} - u_{w(j)}]\frac{\zeta_1 - w(t;t_{(j)})}{w(t;t_{(j+1)}) - w(t;t_{(j)})},$$

$$\text{for } w(t;t_{(j)}) < \zeta_1 < w(t;t_{(j+1)}), \quad (j=\alpha,\alpha+1,\ldots,\alpha'), \tag{26b}$$

where

$$R(x_2,w(t;t_{(j)}),t) = \sum_{m=-N}^{N-1}\int_{q(t,x_2;t_{(j)},-m\Delta x_2)}^{q(t,x_2;t_{(j)},-(m+1)\Delta x_2)} P(x_2,w(t;t_{(j)}),\zeta_2,t)d\zeta_2, \tag{27a}$$

$$P(x_2,w(t;t_{(j)}),\zeta_2,t) = \rho_{w+}(y_2(x_2,w(t;t_{(j)}),\zeta_2,t),t_{(j)})\exp(-\zeta_2^2). \tag{27b}$$

Then, we approximate $\rho_{w+}(y_2(x_2,w(t;t_{(j)}),\zeta_2,t),t_{(j)})$ by a linear function of ζ_2 in each range of integration in Eq. (27a). That is, letting

$$\hat{q}_{(j,m)}(x_2,t) = q(t,x_2;t_{(j)},-m\Delta x_2), \tag{28}$$

and noting that

$$y_2(x_2,w(t;t_{(j)}),\hat{q}_{(j,m)}(x_2,t),t) = -m\Delta x_2, \tag{29}$$

we put

$$\rho_{w+}(y_2(x_2,w(t;t_{(j)}),\zeta_2,t),t_{(j)}) = \rho_{w+}(-m\Delta x_2,t_{(j)}) + [\rho_{w+}(-(m+1)\Delta x_2,t_{(j)}) - \rho_{w+}(-m\Delta x_2,t_{(j)})]\frac{\zeta_2 - \hat{q}_{(j,m)}}{\hat{q}_{(j,m+1)} - \hat{q}_{(j,m)}},$$

$$\text{for } q(t,x_2;t_{(j)},-m\Delta x_2) < \zeta_2 < q(t,x_2;t_{(j)},-(m+1)\Delta x_2), \quad (m=-N,\ldots,0,\ldots,N-1). \tag{30}$$

With these linear approximations in ζ_1 and ζ_2, the integral in Eq. (24) for each j can be expressed in terms of the error function. By summing up the results for j, we can compute Eq. (24) or Eq. (23). Thus, we can compute the integrals containing g_{w+} in Eq. (16) at $t=t_{(i+1)}$ and $x_2=x_{2(l)}$.

Here, we should note the following. If the trajectory $x_1 = x_w(t')$ ($t' \in [0,t]$) is convex upward at t in the x_1t plane as in Fig. 4, then $t_{(\alpha')}$ for $c=n_+$ becomes $t_{(\alpha')}(=s_c^{+'})=t_{(i+1)}$ (see Fig. 4, where $n_+=2$). Thus, the integral from $w(t;t_{(\alpha')})$ to $w(t;s_c^{+'})$ in Eq. (24) vanishes, and the upper limit of the integral for $j=\alpha'-1$ in the same equation becomes $\lim_{\epsilon(>0)\to 0} w(t_{(i+1)};t_{(i+1)}-\epsilon)$. But in consistency with the linear approximation in Eq. (22a), we should assume $x_w(t_{(i+1)} - \epsilon) = x_{w(i)} + u_{w(i)}(\Delta t - \epsilon)$, so that it follows from Eqs. (13) and (22a) that $\lim_{\epsilon(>0)\to 0} w(t_{(i+1)};t_{(i+1)}-\epsilon)=u_{w(i)}$ [we should interpret that $\lim_{\epsilon(>0)\to 0} w(t_{(i+1)};t_{(i+1)}+\epsilon)=u_{w(i+1)}$]. On the other hand, the lower limit of the integral in Eq. (24) for $j = \alpha'-1$ becomes $w(t_{(i+1)};t_{(i)})$, which reduces to $u_{w(i)}$ by the use of Eqs. (13) and (22a). Therefore, the integral for $j=\alpha' - 1$ in Eq. (24) vanishes. In this way, we get rid of $\rho_{w+}(\cdot,t_{(i+1)})$, which is unknown, from the numerical computation of the right-hand side of Eq. (16) at $t=t_{(i+1)}$ and $x_2 = x_{2(l)}$.

When the velocity of the plate u_w approaches the final velocity $u_{w\infty}$, the trajectory $x_1=x_w(t)$ becomes almost a straight line. Suppose that it approaches the straight line from below in the x_1t plane. For $c=n_+$ and for large j, the $w(t_{(i+1)};t_{(j)})$, appearing as the limits of the range of integrals in Eq. (24), becomes almost the same as the plate velocity $u_{w(i)}$. In this case, many integrals under the summation in Eq. (24) can be replaced by a single integral over a much wider integration range.

In this way, we obtain $\rho_{w+}(x_{2(l)},t_{(i+1)})$. Similarly, by the use of Eq. (18), we can obtain $\rho_{w-}(x_{2(l)},t_{(i+1)})$. With these quantities, $G_{\pm}(t_{(i+1)})$ are obtained by the discretized versions of Eqs. (19) and (20). In this process, the integrals under $\Sigma_{c=1}^{n_+}$ and $\Sigma_{c=1}^{n_-}$ in Eqs. (19) and (20) are computed in the same way as in the case of Eq. (16) that have been explained above. The only difference is that $[\zeta_1-u_w(t)]$ in the integrand in Eq. (16) is replaced by $[\zeta_1-u_w(t)]^2$ in Eqs. (19) and (20). The additional integration with respect to x_2 in Eqs. (19) and (20) is carried out by the Simpson rule.

Starting from $i=0$, we can determine the sequence $\{x_{w(n)},u_{w(n)}\}$ $(n=1,2,\ldots)$ by the use of Eq. (22) until a necessary time is reached. We regard this sequence as the numerical solution of our initial-boundary value problem given by Eqs. (6), (7), (8a)–(8c), (9), (10a), (10b), and (11).

The reduction of the above solution procedure to the spatially one-dimensional problem $(d=1)$, as well as its extension to the three-dimensional problem $(d=3)$, is straightforward.

V. RESULTS OF NUMERICAL ANALYSIS

In the long-time limit $t\to\infty$, the velocity of the plate $u_w(t)$ approaches the final velocity $u_{w\infty}$, for which the drag G acting on the plate counterbalances the external force F. In this situation, $\rho_{w\pm}$ is obtained from Eqs. (16) and (18) by setting $u_w(t)=u_{w\infty}$ and the summation terms (the terms under $\Sigma_{c=1}^{n_+}$ and $\Sigma_{c=1}^{n_-}$) to be zero. We can calculate the drag $G=G_++G_-$ from Eqs. (19) and (20) by using the above $\rho_{w\pm}$ and by setting $u_w(t)=u_{w\infty}$ and the summation terms to be zero. In this way, for given u_{w0} and M, the final velocity $u_{w\infty}$ is determined uniquely by F. In what follows, we take $u_{w\infty}$ rather than F as a parameter, so that the dimensionless parameters characterizing the problem are u_{w0}, $u_{w\infty}$, and M [see Eq. (4)]. In addition, we set $M=1$ in this section, in consistency with Refs. [8–11]. This might look unphysical because M should be quite large for a standard solid. However, for the one-dimensional problem, the result for a given M (and given u_{w0} and $u_{w\infty}$) can be obtained from that for $M=1$ (and for the same u_{w0} and $u_{w\infty}$) just by changing the scales of t and x_1 by M (see Sec. V A). More specifically, u_w and ρ_w at $t=\bar{t}$ for $M=\bar{M}$ are given by u_w and ρ_w at $t=\bar{M}\bar{t}$ for $M=1$. For the two- and three-dimensional problem, since the change of the scale by M also applies to x_2 and x_3, the result for $M=1$ corresponds to that for $M\neq 1$ for a plate with a size shrunk by M. In the two-dimensional problem, for instance, u_w and ρ_w at $t=\bar{t}$ for $M=\bar{M}$ for the plate with width 1 are given by u_w and ρ_w at $t=\bar{M}\bar{t}$ for $M=1$ for the plate with width $\bar{M}$. In any case, the assumption $M=1$ does not harm any essential feature of the problem.

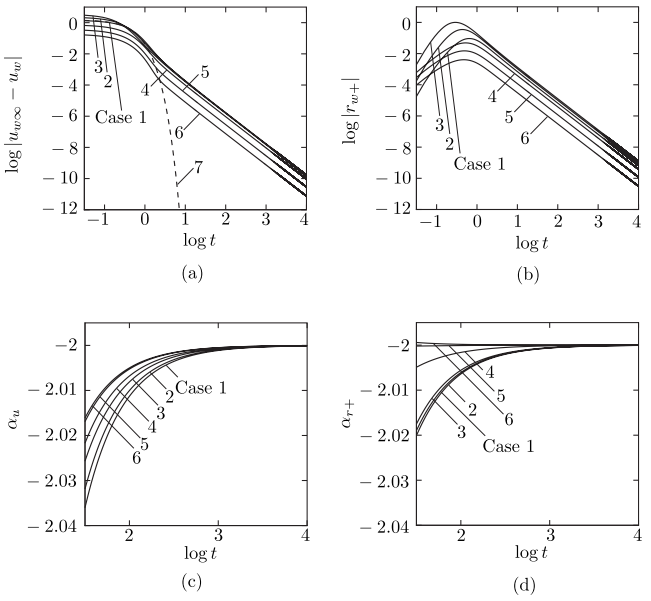

FIG. 5. Long-time behavior for $0\leq u_{w0}<u_{w\infty}$ (one-dimensional problem). (a) $\log|u_{w\infty}-u_w|$ vs $\log t$, (b) $\log|r_{w+}|$ vs $\log t$, (c) α_u vs $\log t$, and (d) α_{r+} vs $\log t$, where $\log(\cdot)$ is the common logarithm $[\log(\cdot)=\log_{10}(\cdot)]$.

In what follows, we will present the results of numerical analysis for the cases of $d=1$, 2, and 3 separately. In addition, some remarks on the numerical computation, including the discussions on the accuracy, will be given in Sec. V D. Our main concern is the time evolution of the velocity $u_w(t)$ of the plate, or more specifically, the decay rate of $u_{w\infty}-u_w(t)$, for long time $t\gg 1$. Moreover, one can infer from the analysis in [11] that the quantities $r_{w+}(t)=G_+(t)-G_{0+}(t)$ and/or $r_{w-}(t)=G_-(t)-G_{0-}(t)$ have similar long-time behavior as $u_{w\infty}-u_w(t)$. Here, $G_{0\pm}(t)$ is the drag acting on the left and right sides of the plate when the effect of recollision is neglected, i.e.,

TABLE I. Values of $\alpha_u(t)$ at large times (one-dimensional problem).

		$-\alpha_u$					
t	$\log t$	Case 1	Case 2	Case 3	Case 4	Case 5	Case 6
31.62	1.5	2.036055	2.031885	2.025712	2.016124	2.016933	2.016124
100.00	2.0	2.011302	2.010035	2.008112	2.004999	2.005267	2.004999
316.23	2.5	2.003564	2.003168	2.002563	2.001571	2.001657	2.001571
1000.00	3.0	2.001126	2.001001	2.000810	2.000496	2.000523	2.000496
3162.28	3.5	2.000356	2.000316	2.000256	2.000157	2.000165	2.000157
10000.00	4.0	2.000113	2.000100	2.000081	2.000048	2.000052	2.000048

TABLE II. Value of $\alpha_{r+}(t)$ at large times (one-dimensional problem).

		$-\alpha_{r+}$					
t	$\log t$	Case 1	Case 2	Case 3	Case 4	Case 5	Case 6
31.62	1.5	2.018999	2.020111	2.017545	2.004910	2.000202	1.999407
100.00	2.0	2.006094	2.006417	2.005585	2.001617	2.000090	1.999824
316.23	2.5	2.001935	2.002034	2.001769	2.000518	2.000031	1.999945
1000.00	3.0	2.000613	2.000644	2.000560	2.000164	2.000010	1.999983
3162.28	3.5	2.000194	2.000204	2.000177	2.000052	2.000003	1.999995
10000.00	4.0	2.000061	2.000064	2.000056	2.000016	2.000001	1.999998

$$G_{0\pm}(t) = \pm \frac{1}{M}\int_{-1/2}^{1/2}\left\{\int_{-\infty}^{\infty}\int_{\zeta_1-u_w(t)\lessgtr 0}[\zeta_1-u_w(t)]^2 \times g_0(\zeta_1,\zeta_2)d\zeta_1 d\zeta_2 + \int_{-\infty}^{\infty}\int_{\zeta_1-u_w(t)\gtrless 0} \times[\zeta_1-u_w(t)]^2\pi^{-1}\rho_{w0\pm}(t)\exp(-[\zeta_1-u_w(t)]^2 - \zeta_2^2)d\zeta_1 d\zeta_2\right\}dx_2, \tag{31a}$$

$$\rho_{w0\pm}(t) = \mp 2\sqrt{\pi}\int_{-\infty}^{\infty}\int_{\zeta_1-u_w(t)\lessgtr 0}[\zeta_1-u_w(t)]g_0(\zeta_1,\zeta_2)d\zeta_1 d\zeta_2, \tag{31b}$$

with the correct solution $u_w(t)$ inserted. We will also show the behavior of these quantities. We also introduce the following auxiliary quantities:

$$\alpha_u = \frac{d\log|u_{w\infty}-u_w(t)|}{d\log t}, \quad \alpha_{r\pm} = \frac{d\log|r_{w\pm}(t)|}{d\log t}, \tag{32}$$

where $\log(\cdot)$ is the common logarithm $[\log(\cdot)=\log_{10}(\cdot)]$. Corresponding to the long-time behavior (1) and (2), we have $\alpha_u \approx -Ct$ (C is a constant) and $\alpha_u \approx -n$, respectively.

For large t, $|u_{w\infty}-u_w(t)|$ becomes very small and loses accuracy because of the cancellation error. Even if it keeps the accuracy of, say three figures, it becomes very difficult to obtain accurate values of the derivative α_u by a finite difference applied to local values of $\log|u_{w\infty}-u_w|$. To avoid this difficulty, we calculate α_u and $\alpha_{r\pm}$ in the following manner. Let $\eta=\log t$ and let us consider the interval $m\le\eta<m+1$ (m: integer). We divide this interval into 100 small sections with the grid points $\eta_j=m+0.01j$ ($j=0,1,2,\ldots,99$). Then, we associate each grid point $\eta=\eta_j$ with an interval $I_j=[\eta_j-0.005,\eta_j+0.005]$. On the basis of the data points of $\log|u_{w\infty}-u_w(t)|$ [or $\log|r_{w\pm}(t)|$] contained in I_j, we obtain a linear function of η using the least-squares method and regard its gradient as α_u (or $\alpha_{r\pm}$) at $\eta=\eta_j$. Since the standard

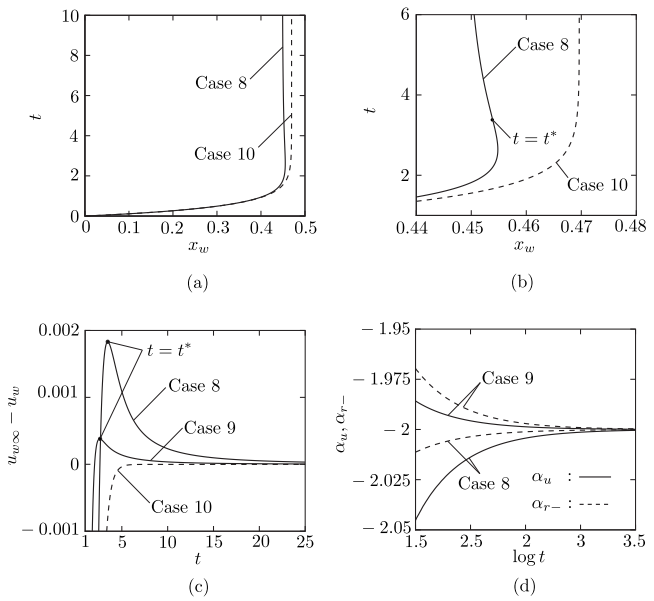

FIG. 6. Time evolution for $0\le u_{w0}<u_{w\infty}$ (one-dimensional problem). (a) Trajectory $x_1=x_w(t)$, (b) magnified figure of (a), (c) $u_{w\infty}-u_w(t)$ vs t, (d) α_u and α_{r-} vs $\log t$.

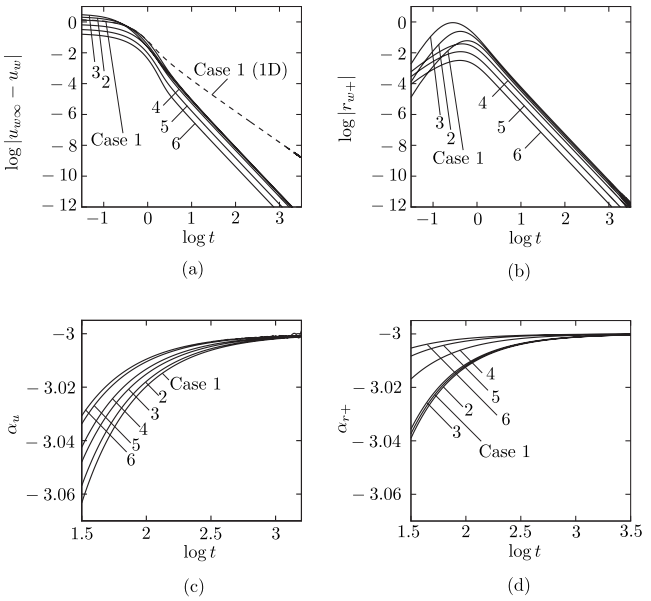

FIG. 7. Long-time behavior for $0\le u_{w0}<u_{w\infty}$ (two-dimensional problem). (a) $\log|u_{w\infty}-u_w|$ vs $\log t$, (b) $\log|r_{w+}|$ vs $\log t$, (c) α_u vs $\log t$, and (d) α_{r+} vs $\log t$.

TABLE III. Values of $\alpha_u(t)$ at large times (two-dimensional problem).

		$-\alpha_u$					
t	$\log t$	Case 1	Case 2	Case 3	Case 4	Case 5	Case 6
31.62	1.5	3.063329	3.056900	3.048011	3.042502	3.033773	3.030717
100.00	2.0	3.019708	3.017834	3.015121	3.013234	3.010493	3.009530
316.23	2.5	3.006203	3.005624	3.004769	3.004169	3.003297	3.003054
1000.00	3.0	3.001961	3.001778	3.001516	3.001286	3.000979	3.000809

time step in the present computation is $\Delta t=0.01$, there are many data points in each I_j for large t.

A. One-dimensional problem

We start with the 1D problem ($d=1$), where the plate is an infinitely wide plate in the x_2x_3 plane. In this case, the reference length L and the reference time τ_0 should be defined as arbitrary numbers satisfying the relation $\tau_0=L(2kT_0/m_*)^{-1/2}$. Therefore, we can choose them in such a way that $M=1$.

We first consider the case of $0\leq u_{w0}<u_{w\infty}$. Figure 5 shows the results for various values of the parameters $(u_{w\infty},u_{w0})$: more specifically, $\log|u_{w\infty}-u_w(t)|$ vs $\log t$ is shown in Fig. 5(a), $\log|r_{w+}(t)|$ vs $\log t$ in Fig. 5(b), α_u vs $\log t$ in Fig. 5(c), and α_{r+} vs $\log t$ in Fig. 5(d) for the following values of the parameters:

$$\text{case 1:}\quad (u_{w\infty},u_{w0})=(1.5,0),$$

$$\text{case 2:}\quad (u_{w\infty},u_{w0})=(2.358\ 15,0),$$

$$\text{case 3:}\quad (u_{w\infty},u_{w0})=(3.556\ 59,0),$$

$$\text{case 4:}\quad (u_{w\infty},u_{w0})=(1.5,0.75),$$

$$\text{case 5:}\quad (u_{w\infty},u_{w0})=(1.5,1.125),$$

$$\text{case 6:}\quad (u_{w\infty},u_{w0})=(1.5,1.3125),$$

$$\text{case 7:}\quad (u_{w\infty},u_{w0})=(1.5,0)\ \text{[no recollision]}.$$

Case 7 is the same as case 1, but the effect of recollision is neglected. Some values of α_u and α_{r+} at large times for case 1 to case 6 are shown in Tables I and II. It is seen from Figs. 5(a) and 5(b) that, in all cases except case 7, $\log|u_{w\infty}-u_w(t)|$ and $\log|r_{w+}(t)|$ seem to become linearly decreasing functions of $\log t$ for t larger than 10. Figures 5(c) and 5(d), together with Tables I and II, demonstrate that the gradients, α_u and α_{r+}, approach -2, which is consistent with Eq. (2) with $n=d+1$, obtained theoretically in [11] under condition (3). On the other hand, in case 7, the approach of $u_w(t)$ to $u_{w\infty}$ is much faster. If $\log|u_{w\infty}-u_w(t)|$ is plotted versus t rather than $\log t$, one can see that the approach is exponential as in Eq. (1). The computation shows that in all the cases, $u_{w\infty}-u_w(t)$ is always positive and decreases monotonically (i.e., the velocity of the plate increases monotonically to the final velocity). In other words, the trajectory $x_1=x_w(t)$ is always convex upward in the x_1t plane, so that $n_+=1$ and $n_-=0$. Incidentally, r_{w+} is always positive (except case 7 for which $r_{w+}=0$), and $r_{w-}=0$.

We next show some results for the case of $0\leq u_{w\infty}<u_{w0}$. Figure 6 contains the results of the following three cases:

$$\text{case 8:}\quad (u_{w\infty},u_{w0})=(0,1),$$

$$\text{case 9:}\quad (u_{w\infty},u_{w0})=(1.5,6),$$

$$\text{case 10:}\quad (u_{w\infty},u_{w0})=(0,1)\ \text{[no recollision]}.$$

Case 10 is the same as case 8 except that the effect of recollision is neglected. Figure 6(a) shows the trajectory $x_1=x_w(t)$ for case 8 (solid line) and case 10 (dashed line) in the x_1t plane (cf. Fig. 4). In these cases the plate stops in the limit $t\to\infty$, since there is no external force. As one can see from the figure, $x_w(t)$ in case 8 does not increase monotonically as time goes on. That is, the plate once exceeds the final position $x_w(\infty)$ slightly and then comes back to it. In contrast, such an overshoot is not observed in case 10. Figure 6(b) is a magnified figure of Fig. 6(a), and Fig. 6(c) shows $u_{w\infty}-u_w(t)$ vs t for the three cases. As seen from Fig. 6(c), the plate velocity $u_w(t)$, which is larger than $u_{w\infty}$ initially, once becomes slightly smaller than $u_{w\infty}$ and then approaches it

TABLE IV. Values of $\alpha_{r+}(t)$ at large times (two-dimensional problem).

		$-\alpha_{r+}$					
t	$\log t$	Case 1	Case 2	Case 3	Case 4	Case 5	Case 6
31.62	1.5	3.037372	3.039033	3.035636	3.016899	3.008318	3.005314
100.00	2.0	3.011864	3.012389	3.011320	3.005424	3.002697	3.001738
316.23	2.5	3.003757	3.003922	3.003585	3.001723	3.000859	3.000555
1000.00	3.0	3.001188	3.001241	3.001134	3.000546	3.000272	3.000176

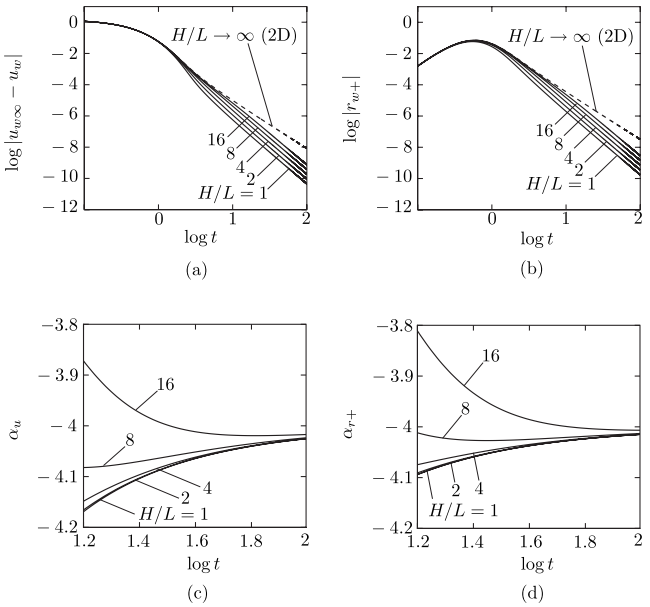

FIG. 8. Long-time behavior for case 1 with various aspect ratios (three-dimensional problem). (a) $\log|u_{w\infty}-u_w|$ vs $\log t$, (b) $\log|r_{w+}|$ vs $\log t$, (c) α_u vs $\log t$, and (d) α_{r+} vs $\log t$.

from below. In cases 8 and 9, the peak of $u_{w\infty}-u_w(t)$ ($u_{w\infty}=0$ in case 8) is attained, respectively, at $t=t^*=3.4775$ and 2.6125, at which the curvature of the trajectory $x_1=x_w(t)$ changes its sign [see Fig. 6(b)]. In contrast, the overshoot of $u_{w\infty}-u_w(t)$ is not observed in case 10 where the effect of recollision is neglected. In Fig. 6(d), α_u and α_{r-} vs $\log t$ are shown for cases 8 and 9. Both of them approach −2. In these cases, $n_+=0$ and $n_-=1$ for $0<t\le t^*$, whereas $n_+=1$ and $n_-=1$ for $t^*<t$. In cases 8 and 9, $|r_{w+}|$ is negligibly small compared to $|r_{w-}|$. The overshoot of the position and the velocity difference $u_{w\infty}-u_w(t)$ have been predicted theoretically in [9] in the case of specular reflection under condition (3).

B. Two-dimensional problem

Next we consider the 2D problem ($d=2$) that is described explicitly in Secs. II–IV. Figure 7 shows the results for case 1 to case 6 (see Sec. V A) in the present 2D problem. The figure corresponds to Fig. 5 for the 1D problem. Some values of α_u and α_{r+} at large times up to $t=10^3$ for case 1 to case 6 are shown in Tables III and IV. In the figure, "case 1 (1D)" indicates the result for case 1 in the 1D problem. As seen from Figs. 7(a)–7(d) and Tables III and IV, both of $\log|u_{w\infty}-u_w(t)|$ and $\log|r_{w+}(t)|$ seem to become linearly decreasing functions, with gradient −3, of $\log t$ for large t. This is consistent with Eq. (2) with $n=d+1$ obtained theoretically under condition (3) in [11]. The results of α_u in Fig. 7(c), in particular those for cases 5 and 6, show oscillation for $\log t$ larger than about 3 (i.e., $t\gtrsim 1000$). The reason for this phenomenon is the following. The decay of $|u_{w\infty}-u_w(t)|$ is faster in the 2D problem and its value becomes smaller than 10^{-11} for t larger than 10^3. This is smaller than the same quantity in the 1D problem by 3 to 4 orders of magnitude, so that it suffers from cancellation errors at earlier times. Because of this factor, the accuracy of the derivative α_u seems to be lost

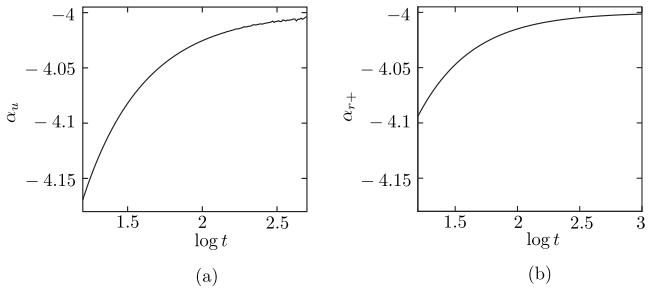

FIG. 9. Long-time behavior for case 1 with $H/L=1$ (square plate) (three-dimensional problem). (a) α_u vs $\log t$, and (b) α_{r+} vs $\log t$.

for $t\gtrsim 1000$ though $|u_{w\infty}-u_w(t)|$ itself is still fairly accurate. The fact that we need to handle the additional x_2 variable in the 2D problem also increases the computational load. For α_{r+} in Fig. 7(d), the oscillation is not observed yet. As in the 1D problem, $u_{w\infty}-u_w(t)$ is positive and decreases monotonically, and we have $n_+=1$, $n_-=0$, $r_{w+}>0$, and $r_{w-}=0$.

C. Three-dimensional problem

Finally we show some results for the three-dimensional (3D) problem ($d=3$), where the plate (without thickness) is a rectangle with sides L and H, located initially at $X_1=0$, $-L/2\le X_2\le L/2$, and $-H/2\le X_3\le H/2$ (or $x_1=0$, $-1/2\le x_2\le 1/2$, and $-H/2L\le x_3\le H/2L$). Figure 8 shows some preliminary results, based on rather coarse grids in x_2 and x_3 (see Sec. V D), for case 1 in Sec. V A for different aspect ratios: $H/L=1$, 2, 4, 8, and 16. As in Figs. 5 and 7, the panels (a), (b), (c), and (d) show $\log|u_{w\infty}-u_w(t)|$, $\log|r_w(t)|$, α_u, and α_{r+} vs $\log t$, respectively. The 2D problem ($H/L\to\infty$) is also shown by the dashed line in Figs. 8(a) and 8(b). It is seen from the figure that α_u and α_{r+} have a tendency to approach −4, which is consistent with the theoretical result, Eq. (2) with $n=d+1$, obtained in [11] under condition (3). However, to see it more clearly, we have to obtain a more accurate numerical solution until much larger t, which requires a very heavy computation. Therefore, we carry out such computation only for $H/L=1$. Figure 9 shows α_u and α_{r+} vs $\log t$ obtained by this computation and Table V gives the corresponding numerical values at long times. It is seen from Fig. 9 and Table V that α_u and α_{r+} tend to approach −4. In Fig. 9(a), an oscillation, similar to that in Fig. 7(c), is observed before $\log t=2.5$ ($t=316$). As in the 1D and 2D problems, $u_{w\infty}-u_w(t)$ is always positive and decreases monotonically,

TABLE V. Values of $\alpha_u(t)$ and $\alpha_{r+}(t)$ at large times for case 1 with $H/L=1$ (square plate) (three-dimensional problem).

t	$\log t$	$-\alpha_u$	$-\alpha_{r+}$
15.85	1.2	4.169216	4.094073
31.62	1.5	4.082090	4.047232
100.00	2.0	4.025448	4.014949
316.23	2.5	4.008078	4.004729
1000.00	3.0	⋯	4.001496

TABLE VI. Values of $u_\infty - u_w(t)$ for case 1 with different Δt (one-dimensional problem).

		$u_\infty - u_w(t)$						
t	$\log t$	$\Delta t=0.1$	$\Delta t=0.05$	$\Delta t=0.02$	$\Delta t=0.01$	$\Delta t=0.005$	$\Delta t=0.002$	$\Delta t=0.001$
1	0.0	4.9198×10^{-2}	5.8070×10^{-2}	6.2945×10^{-2}	6.4500×10^{-2}	6.5265×10^{-2}	6.5720×10^{-2}	6.5871×10^{-2}
5	0.7	5.9364×10^{-4}	7.2347×10^{-4}	8.0840×10^{-4}	8.3765×10^{-4}	8.5243×10^{-4}	8.6135×10^{-4}	8.6433×10^{-4}
10	1.0	1.3178×10^{-4}	1.6031×10^{-4}	1.7893×10^{-4}	1.8533×10^{-4}	1.8856×10^{-4}	1.9051×10^{-4}	1.9116×10^{-4}
50	1.7	4.8105×10^{-6}	5.8464×10^{-6}	6.5211×10^{-6}	6.7529×10^{-6}	6.8699×10^{-6}	6.9404×10^{-6}	6.9639×10^{-6}
100	2.0	1.1892×10^{-6}	1.4451×10^{-6}	1.6118×10^{-6}	1.6690×10^{-6}	1.6979×10^{-6}	1.7153×10^{-6}	1.7212×10^{-6}
500	2.7	4.7144×10^{-8}	5.7286×10^{-8}	6.3889×10^{-8}	6.6157×10^{-8}	6.7301×10^{-8}	6.7996×10^{-8}	6.8221×10^{-8}
1000	3.0	1.1773×10^{-8}	1.4305×10^{-8}	1.5954×10^{-8}	1.6520×10^{-8}	1.6806×10^{-8}	1.6978×10^{-8}	1.7036×10^{-8}

TABLE VII. Values of $\alpha_u(t)$ for case 1 with different Δt (one-dimensional problem).

		$-\alpha_u$						
t	$\log t$	$\Delta t=0.1$	$\Delta t=0.05$	$\Delta t=0.02$	$\Delta t=0.01$	$\Delta t=0.005$	$\Delta t=0.002$	$\Delta t=0.001$
31.62	1.5	2.032576	2.034489	2.035645	2.036055	2.036443	2.036470	2.036479
100.00	2.0	2.010204	2.010803	2.011176	2.011302	2.011416	2.011424	2.011427
316.23	2.5	2.003216	2.003407	2.003523	2.003564	2.003599	2.003602	2.003603
1000.00	3.0	2.001017	2.001076	2.001113	2.001126	2.001137	2.001138	2.001138

TABLE VIII. Values of $u_\infty - u_w(t)$ for case 1 with different Δx_2 (two-dimensional problem).

		$u_\infty - u_w(t)$		
t	$\log t$	$\Delta x_2=1/14$	$\Delta x_2=1/30$	$\Delta x_2=1/62$
1	0.0	5.901367×10^{-2}	5.901460×10^{-2}	5.901480×10^{-2}
5	0.7	9.972841×10^{-5}	9.973847×10^{-5}	9.974059×10^{-5}
10	1.0	9.949553×10^{-6}	9.950565×10^{-6}	9.950777×10^{-6}
50	1.7	6.747572×10^{-8}	6.748259×10^{-8}	6.748403×10^{-8}
100	2.0	8.268005×10^{-9}	8.268846×10^{-9}	8.269023×10^{-9}
500	2.7	6.510437×10^{-11}	6.511103×10^{-11}	6.511236×10^{-11}
1000	3.0	8.121948×10^{-12}	8.122836×10^{-12}	8.123058×10^{-12}

TABLE IX. Values of $\alpha_u(t)$ for case 1 with different Δx_2 (two-dimensional problem).

		$-\alpha_u$		
t	$\log t$	$\Delta x_2=1/14$	$\Delta x_2=1/30$	$\Delta x_2=1/62$
31.62	1.5	3.063329	3.0633287	3.0633287
100.00	2.0	3.019708	3.0197084	3.0197083
316.23	2.5	3.006202	3.0062039	3.0062040
1000.00	3.0	3.001961	3.0019547	3.0019512

and we have $n_+=1$, $n_-=0$, $r_{w+}>0$, and $r_{w-}=0$ for all the cases in Figs. 8 and 9.

D. Remarks on numerical computation

In the present computation, we have restricted ourselves to the case of the diffuse reflection rather than the specular reflection. The first reason is that the case of the specular reflection is more tractable mathematically, so that more rigorous results are available [8–10]. Therefore, studying the case of the diffuse reflection is more complementary. The second and main reason is that the computation is more difficult for the specular reflection. For the diffuse reflection, we need to store only $x_w(t_{(j)})$, $u_w(t_{(j)})$, and $\rho_{w\pm}(x_{2(l)},t_{(j)})$ at all $t_{(j)}$, from which we can compute the velocity distribution function of the molecules leaving the plate. In contrast, for the specular reflection, we have to either store the velocity distribution function of the leaving molecules at all $t_{(j)}$ or trace back, at each $t_{(i)}$, the trajectories of the recolliding molecules until the initial distribution is reached. These processes, which are memory-consuming or time-consuming, make a long-time computation formidable.

In the computation for Figs. 5 and 6(d) in the 1D problem, we have set $\Delta t=0.01$. However, for Figs. 6(a)–6(c), which require very accurate computation at short times, we used a smaller time step $\Delta t=0.005$. We have also examined the effect of the time step Δt on the solution for case 1. Some results are shown in Tables VI and VII. Table VI shows the values of $u_\infty-u_w(t)$ at different times for $\Delta t=0.1$, 0.05, 0.02, 0.01, 0.005, 0.002, and 0.001, and Table VII the values of α_u at large times for the same Δt's. Table VI clearly shows the fact that our finite-difference scheme (22) is of first order in Δt. According to the same table, we need $\Delta t=0.01$ to obtain the accuracy of 3% relative error and $\Delta t=0.005$ the accuracy of 1.5% relative error. However, Table VII shows that the decay exponent α_u is much less sensitive to Δt and that $\Delta t=0.01$ is sufficient to obtain accurate values of α_u.

The 2D computation for the data in Fig. 7 was performed with $\Delta t=0.01$ and $\Delta x_2=1/14$. Here, we have checked the effect of Δx_2 on the solution with finer grid points, $\Delta x_2=1/30$ and 1/62, for case 1. Some results are shown in Tables VIII and IX. To be more specific, Table VIII shows $u_\infty-u_w(t)$ at different times for $\Delta x_2=1/14$, 1/30, and 1/62, and Table IX the corresponding values of α_u at some large times. As seen from these tables, $\Delta x_2=1/14$ gives a sufficiently accurate result.

The 3D computation, which is much heavier than 2D computation, prevents from using fine grid points in x_2 and x_3. Therefore, we have used $\Delta t=0.01$ and $\Delta x_2=\Delta x_3=1/6$ [i.e., $7\times 7(H/L)$ points on the plate] for the preliminary result shown in Fig. 8, where Δx_3 is the grid size in the x_3 direction. However, in order to establish the reliable long-time behavior, we carried out a computation with finer grid points in x_2 and x_3 for the square plate ($H/L=1$, case 1), i.e., a computation with $\Delta t=0.01$ and $\Delta x_2=\Delta x_3=1/14$. Figure 9 demonstrates such a result. In this connection, we have carried out the same computation with larger time steps, $\Delta t=0.1$, 0.05, and 0.02, to see the effect of the time step. The results are shown in Tables X and XI.

The computation was carried out with quadruple precision. If we perform the 2D computation with double precision, the strong oscillation exhibited in Fig. 7(c) appears at much earlier times. It should be mentioned that we have employed a fast algorithm for the error function provided by Ooura, available from his home page (http://www.kurims.kyoto-u.ac.jp/~ooura/index.html). The algorithm is for double precision, but we have confirmed that it gives an accuracy of 19 significant figures if it is used in a quadruple-precision computation.

The computation has been carried out on a personal computer with CPU: Intel(R) Xeon(R) X5355 2.66GHz×8.

VI. CONCLUDING REMARKS

In this paper we have investigated numerically an unsteady motion of a plate in a free-molecular gas at rest

TABLE X. Values of $u_\infty-u_w(t)$ for case 1 ($H/L=1$) with different Δt (three-dimensional problem).

		$u_\infty-u_w(t)$			
t	$\log t$	$\Delta t=0.1$	$\Delta t=0.05$	$\Delta t=0.02$	$\Delta t=0.01$
1	0.0	4.1660×10^{-2}	4.9610×10^{-2}	5.3867×10^{-2}	5.5210×10^{-2}
5	0.7	8.7286×10^{-6}	1.0632×10^{-5}	1.1883×10^{-5}	1.2317×10^{-5}
10	1.0	4.1238×10^{-7}	4.9498×10^{-7}	5.4796×10^{-7}	5.6604×10^{-7}
50	1.7	5.3709×10^{-10}	6.4109×10^{-10}	7.0732×10^{-10}	7.2982×10^{-10}
100	2.0	3.2744×10^{-11}	3.9065×10^{-11}	4.3088×10^{-11}	4.4454×10^{-11}
500	2.7	5.1292×10^{-14}	6.1284×10^{-14}	6.7502×10^{-14}	6.9722×10^{-14}
1000	3.0	3.1086×10^{-15}	3.7748×10^{-15}	4.2188×10^{-15}	4.4409×10^{-15}

TABLE XI. Values of $\alpha_u(t)$ for case 1 ($H/L=1$) with different Δt (three-dimensional problem).

		$-\alpha_u$			
t	$\log t$	$\Delta t=0.1$	$\Delta t=0.05$	$\Delta t=0.02$	$\Delta t=0.01$
15.85	1.2	4.149665	4.160207	4.166830	4.169216
31.62	1.5	4.073104	4.077973	4.081020	4.082090
100.00	2.0	4.022755	4.024270	4.025114	4.025448
158.49	2.2	4.013993	4.015431	4.015819	4.015973

caused by a uniform external force and by a drag exerted by the gas molecules, with special interest in the rate of approach to the final steady motion. The study complements the preceding mathematical results [8–11] on a similar problem (a circular disk or general convex body, rather than a plate, was considered in these works) that showed a slow approach in proportion to some inverse power of time. In these works it was also revealed that the slow approach is caused by the fact that some of the molecules that have been reflected by the body in the past are hit by the body again (recollision). The theoretical results, however, are based on the assumption that the initial velocity of the body is very close to its final velocity. In the present study we were able to provide some numerical evidences, in the case of diffuse reflection studied in [11], that the same result holds when the initial velocity of the body is quite different from the final velocity.

The motion of a body in a free-molecular gas is encountered in connection with the motion of nanoscale aerosol particles, that of satellites or spacecrafts, etc. When the motion is unsteady and undergoes acceleration, deceleration, rotation, etc., one expects that the gas molecules keep a memory from the initial stage because of the absence of intermolecular collisions that destroy the memory, and this fact may affect the motion of the body at later times. The present study, as well as the previous studies [8–11], clarifies the basic properties of the effect of long memory, which manifests itself in the form of recollision of the molecules. There are some interesting studies of migrations of a convex body in a free-molecular gas caused by various kinds of forces (thermophoresis, shearing phoresis, etc.) [17–19]. However, in spite of the fact that these migrations contain unsteady motions of the body, the effect of recollision is not taken into account in these works. That is, the distribution function of the gas molecules impinging on the body is assumed to be given by that at infinity at any instant. If the effect of recollision is taken into account, it may change the trajectory of the body significantly. The present study provides a step to tackle such problems.

ACKNOWLEDGMENTS

The authors thank Professor Carlo Marchioro and Professor Mario Pulvirenti for their valuable discussions. Thanks are also due to Professor Shigeru Takata for his helpful comments. The work was supported by the Grant-in-Aid for Scientific Research (Grant No. 20360046) from JSPS.

[1] H. Grad, in *Handbuch der Physik*, edited by S. Flügge (Springer, Berlin, 1958), Vol. XII, pp. 205–294.
[2] M. N. Kogan, *Rarefied Gas Dynamics* (Plenum, New York, 1969).
[3] C. Cercignani, *The Boltzmann Equation and Its Applications* (Springer, New York, 1988).
[4] C. Cercignani, R. Illner, and M. Pulvirenti, *The Mathematical Theory of Dilute Gases* (Springer, New York, 1994).
[5] Y. Sone, *Kinetic Theory and Fluid Dynamics* (Birkäuser, Boston, 2002).
[6] Y. Sone, *Molecular Gas Dynamics: Theory, Techniques, and Applications* (Birkäuser, Boston, 2007).
[7] S. A. Schaaf and P. L. Chambré, in *Fundamentals of Gas Dynamics*, edited by H. W. Emmons (Princeton University Press, Princeton, 1958), Chap. H.
[8] S. Caprino, C. Marchioro, and M. Pulvirenti, Commun. Math. Phys. **264**, 167 (2006).
[9] S. Caprino, G. Cavallaro, and C. Marchioro, Math. Models Meth. Appl. Sci. **17**, 1369 (2007).
[10] G. Cavallaro, Rendiconti di Matematica, Ser. VII **27**, 123 (2007).
[11] K. Aoki, G. Cavallaro, C. Marchioro, and M. Pulvirenti, Math. Modell. Numer. Anal. **42**, 263 (2008).
[12] V. Balakrishnan, I. Bena, and C. Van den Broeck, Phys. Rev. E **65**, 031102 (2002).
[13] C. Gruber and J. Piasecki, Physica A **268**, 412 (1999).
[14] J. L. Lebowitz, J. Piasecki, and Y. Sinai, in *Hard Ball Systems and the Lorentz Gas*, Encyclopedia of Mathematical Sciences Vol. 101 (Springer, New York, 2000), pp. 217–227.
[15] P. Buttà, E. Caglioti, and C. Marchioro, J. Stat. Phys. **108**, 317 (2002).
[16] P. Buttà, E. Caglioti, and C. Marchioro, Commun. Math. Phys. **233**, 545 (2003).
[17] K. I. Borg, Ph.D. thesis, Royal Institute of Technology, Stockholm, Sweden, 2003.
[18] K. I. Borg and L. H. Söderholm, *Rarefied Gas Dynamics*, edited by T. J. Bartel and M. A. Gallis (AIP, Melville, 2001), pp. 867–874.
[19] K. I. Borg and L. H. Söderholm, Eur. J. Mech. B/Fluids **27**, 623 (2008).